Lineage-specific patterns in the Moraceae family allow identification of convergent P450 enzymes involved in furanocoumarin biosynthesis

New Phytologist

Bouillé, Alexandre; Larbat, Romain; Kumari, Rashmi; Olry, Alexandre; Charles, Clément et al

https://doi.org/10.1111/nph.20381

New Phytologist

Research

Lineage-specific patterns in the Moraceae family allow identification of convergent P450 enzymes involved in furanocoumarin biosynthesis

Alexandre Bouillé[1], Romain Larbat[2], Rashmi Kumari[3], Alexandre Olry[1], Clément Charles[1], David R. Nelson[4], Janet Thornton[3], Cloé Villard[5]* and Alain Hehn[1]*

[1]Université de Lorraine, INRAE, LAE, 54000, Nancy, France; [2]Institut Agro, University of Angers, INRAE, IRHS, SFR QUASAV, F-49000, Angers, France; [3]European Bioinformatics Institute (EMBL-EBI), Wellcome Genome Campus, CB10 1SD, Cambridge, UK; [4]Department of Microbiology, Immunology and Biochemistry, University of Tennessee Health Science Center, Memphis 38163 TN, USA; [5]Biosystematics Group, Wageningen University and Research, Wageningen, 6708 PB, the Netherlands

Author for correspondence:
Alain Hehn
Email: alain.hehn@univ-lorraine.fr

Received: *19 August 2024*
Accepted: *10 December 2024*

New Phytologist (2025)
doi: 10.1111/nph.20381

Key words: coumarins, cytochrome P450, enzyme functional convergence, furanocoumarins, Moraceae, specialized metabolism.

Summary

- Specialized metabolites are molecules involved in plants' interaction with their environment. Elucidating their biosynthetic pathways is a challenging but rewarding task, leading to societal applications and ecological insights. Furanocoumarins emerged multiple times in Angiosperms, raising the question of how different enzymes evolved into catalyzing identical reactions.
- To identify enzymes producing lineage-specific metabolites, an evolutionary-based approach was developed and applied to furanocoumarin biosynthesis in *Ficus carica* (Moraceae). This led to the characterization of CYP71B129–131a, three P450 enzymes whose evolution of the function was investigated using phylogenetics, structural comparisons and site-directed mutagenesis.
- CYP71B129 and CYP71B130,131a were found to hydroxylate umbelliferone (coumarin) and xanthotoxin (furanocoumarin), respectively. Results suggest that CYP71Bs xanthotoxin hydroxylase activity results from duplications and functional divergence of umbelliferone hydroxylase genes. Structural comparisons highlighted an amino acid affecting CYP71Bs substrate specificity, which may play a key role in allowing xanthotoxin hydroxylation in several P450 subfamilies.
- CYP71B130-131a characterization validates the proposed enzyme-discovery approach, which can be applied to different pathways and help to avoid the classic bottlenecks of specialized metabolism elucidation. The CYP71Bs also exemplify how furanocoumarin-biosynthetic enzymes can stem from coumarin-biosynthetic ones and provides insights into the molecular mechanisms underlying the multiple emergences of xanthotoxin hydroxylation in distant P450 subfamilies.

Introduction

To adapt to their environment, plants have evolved various strategies including a large metabolic expansion which led to the production of myriads of molecules called plant specialized metabolites (PSMs) (Ono & Murata, 2023). Overall, the plant kingdom produces millions of structurally different PSMs, and each plant lineage possesses a unique metabolic profile. Remarkably, distant plants can produce similar PSMs, but rely on different enzymes to synthesize them. This phenomenon of convergent evolution toward an identical function is very common in specialized metabolism, making the biosynthesis of a given PSM potentially unique in each plant (Pichersky & Lewinsohn, 2011). Hence, PSM biosynthesis pathways are generally challenging to elucidate. To identify enzymes involved in PSM biosynthesis, various approaches were developed, relying on strategies such as sequence homology search, transcriptomic analyses, or gene mapping. For instance, it is common to analyze PSMs' accumulation patterns (e.g. tissues distribution, stress inducibility) to identify candidate enzymes displaying correlated gene expression (Ono & Murata, 2023). Such strategies are efficient and have already been successfully used, but they can be limited by factors such as low metabolite or transcription levels or recent divergent and convergent evolution (Pichersky & Lewinsohn, 2011). Promising advanced bioinformatic approaches such as deep learning and large-scale docking are also being developed, but still have limited efficiency (Daniel *et al.*, 2015; Moore *et al.*, 2019).

*These authors shared last authorship.

Furanocoumarins are a class of defensive PSM effective against various bioaggressors such as pathogens and phytophagous insects (Stevenson *et al.*, 2003). Although derived from ubiquitous coumarins, furanocoumarins have only been identified in a few phylogenetically distant plant lineages including the Apiaceae, Rutaceae, Fabaceae and Moraceae (Sarker & Nahar, 2017). Over the past decades, the furanocoumarin biosynthesis pathway has been significantly elucidated in Apiaceous, Rutaceous and Moraceous species (Fig. 1). This pathway involves enzymes from the 2-oxoglutarate-dependent dioxygenase (Roselli *et al.*, 2017), prenyltransferase (Munakata *et al.*, 2020), O-methyltransferase (Hehmann *et al.*, 2004), and cytochrome P450 (P450) families (Villard *et al.*, 2021) (Fig. 1). Interestingly, identifying furanocoumarin-biosynthetic enzymes from different species showed that furanocoumarins are a case of convergent evolution: they emerged independently in distant plant lineages, in which they are synthesized by different enzymes (Limones-Mendez *et al.*, 2020; Munakata *et al.*, 2020; Villard *et al.*, 2021).

Currently, the most referenced step of the furanocoumarin pathway corresponds to xanthotoxin hydroxylation (Fig. 1), catalyzed by 5-hydroxyxanthotoxin synthases (5OXHSs). All 5OHXSs characterized so far are P450s but belong to different (sub)families. Indeed, 5OHXSs from the Rutaceae (i.e. *Citrus hystrix* and *Citrus paradisi*) are CYP82Ds (Limones-Mendez *et al.*, 2020), while 5OHXS from the Apiaceae (i.e. *Pastinaca sativa*) belong to the CYP71AZs (Krieger *et al.*, 2018). Curiously, CYP82Cs from *Arabidopsis thaliana* (Brassicaceae) also display *in vivo* 5OHXS activity, although *Arabidopsis* does not naturally accumulate furanocoumarins (Kruse *et al.*, 2008).

To pursue the elucidation of furanocoumarin biosynthesis and better understand the evolutionary process underlying the emergence of this pathway, we sought new furanocoumarin-biosynthetic enzymes in *Ficus carica* (Moraceae). To facilitate the identification of enzymes involved in the production of lineage-specific PSMs such as furanocoumarins, we established an evolutionary-based approach. Applying this approach, we compared the CYPomes of two Moraceae: *F. carica*, which produces furanocoumarins, and *Morus notabilis*, which, as far as described, does not. This led to identifying three *F. carica* CYP71Bs displaying 5OHXS and umbelliferone hydroxylase (UMBH) activity. Phylogenetics and comparative structural biology shed light on a lineage-specific diversification and highlighted an important residue which impacts enzyme activity and may have played a key role in the acquisition of the 5OHXS function.

Materials and Methods

Plant material and chemicals

Ficus carica L. plants were provided by INRAE Colmar (France). They were grown for 4 yr at room temperature and under natural light. Standard specimens of phenolic compounds were purchased from various suppliers, as described in Supporting Information Table S1.

Comparison of the CYP71 clan in *F. carica* and *M. notabilis*

A P450 nucleotide dataset was assembled with *F. carica* and *Morus notabilis C. K.* Schneid CYP71 clan sequences (Table S2). *Morus notabilis* sequences were retrieved from Ma *et al.* (2014). *Ficus carica* sequences were identified by screening the PRJNA565858 reference genome (Usai *et al.*, 2020) through BLASTN searches, using *M. notabilis* genes as queries and an e-value of 1000. Resulting hits were used to isolate full-length putative P450 genes and pseudogenes. Introns were predicted and removed using the NETGENE2 Server (http://www.cbs.dtu.dk/services/NetGene2/) (Hebsgaard, 1996). Putative pseudogenes containing frameshifts were altered by the addition of one or two 'N' at the site of the indel(s) to recover a functional reading frame and allow subsequent analyses (Table S2a). *CYP51G* sequences were added to the dataset, to constitute the outgroup of the following tree. Sequences received a standardized name from the P450 nomenclature committee (https://drnelson.uthsc.edu/CytochromeP450.html, Fig. S1). Nucleotide sequences were then translated into proteins and aligned (Fig. S2) with MAAFT v.7 (https://mafft.cbrc.jp/alignment/server/) relying on default parameters (Kuraku *et al.*, 2013; Katoh *et al.*, 2019). Aligned sequences were used to build a Bayesian inference protein tree with MRBAYES v.3.2.7 (Ronquist & Huelsenbeck, 2003; Ronquist *et al.*, 2012) at CIPRES v.3.3 (Cipres Science Gateway). The Bayesian Markov Chain Monte Carlo analysis was run with the following parameters: nst = mixed, rates = gamma, shape = (all), 2 million generations, two independent runs, four chains, temperature heating 0.05. The tree was drawn with FIGTREE v.1.4.4. Posterior probabilities supporting tree-branches were considered weak below 0.7, strong above 0.9.

Cloning of *CYP71B129*, *CYP71B130* and *CYP71B131a* coding sequences

Total RNAs were extracted from young *F. carica* leaves and reverse-transcribed into complementary DNAs as described in Villard *et al.* (2021). *CYP71B129*, *CYP71B130* and *CYP71B131a* coding sequences (CDSs) were PCR-amplified using the PrimeSTAR® Max polymerase (Takara, Saint-Germain-en-Laye, France), according to supplier's recommendations. Associated primers were 5′-GAAGAAAAATCATAGTAGAAATCTGAGT CATAAACTCCA-3′ (forward) and 5′-CAAATTTTTATTCT CTGTTTATATTTCTACTAGAAGATTGTTCAATGCAA-3′ (reverse) for *CYP71B129*, 5′-GGGAATCGAATTAGAAATCT AAGTGATAAGCTCCA-3′ (forward) and 5′-GTTTTTTCT AGAGAAAATTAACAACTTCGCTAACATATGTC-3′ (reverse) for *CYP71B130*, and 5′-GCGAATTGAACTAGAAATCAAA CTGATAAGCTCCA-3′ (forward) and 5′-GTTACTAG TTTTATTTTTGAGAAAACATATTCAAGTCTATTTGAAG AAGTTT-3′ (reverse) for *CYP71B131a*. CDSs were then inserted into the pCR™8/GW/TOPO® TA vector (Invitrogen™, Thermo Fisher Scientific, Illkirch-Graffenstaden, France). Each gene was independently cloned and sequenced twice. A 3′-end 6xHis-tag was added by PCR, using the following primers:

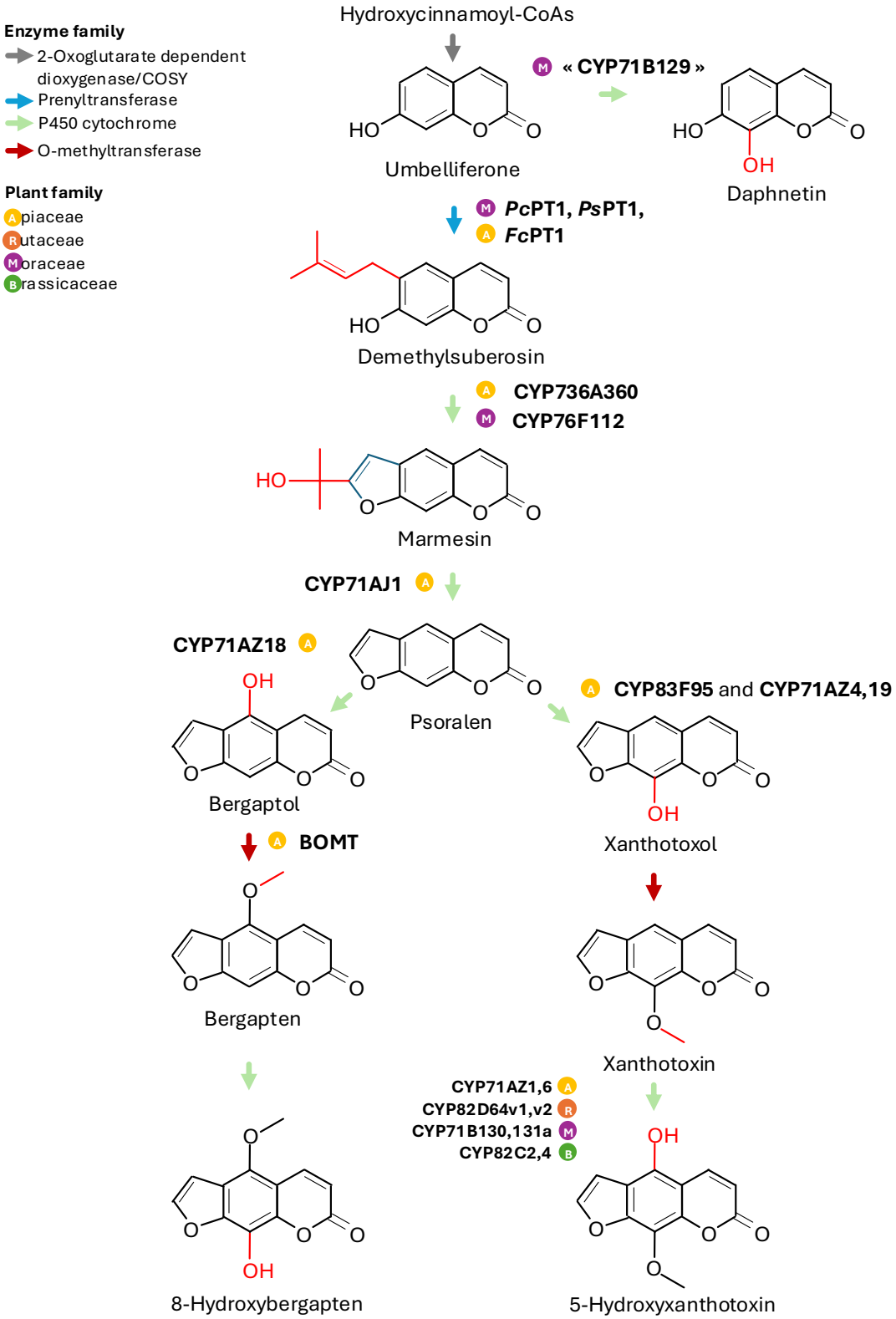

Fig. 1 Simplified representation of the furanocoumarin-biosynthetic pathway in Angiosperms. All furanocoumarin-biosynthetic enzymes described so far are detailed, together with associated plant families (Hehmann *et al*., 2004; Larbat *et al*., 2007; Kruse *et al*., 2008; Karamat *et al*., 2014; Roselli *et al*., 2017; Krieger *et al*., 2018; Limones-Mendez *et al*., 2020; Munakata *et al*., 2020; Villard *et al*., 2021; Ji *et al*., 2024; Wang *et al*., 2024). BOMT, bergaptol O-methyltransferase; FcPT1, *Ficus carica* prenyltransferase 1; PcPT, *Petroselinum crispum* prenyltransferase; PsPT1, *Pastinaca sativa* prenyltransferase 1; XOMT, xanthotoxol O-methyltransferase.

5′-CCAATGGCTATTGATGCCCAAC-3′ (forward) and 5′-CAACTAATGATGATGATGATGGAGGTGCTTCTTTGGGAC-3′ (reverse) for *CYP71B129*, 5′-CCAATGGCTATGGATGCCCAAC-3′ (forward) and 5′-GTTCTAATGATGATGATGATGATGTGCAAATAGGTGCTTCTTTG-3′ (reverse) for *CYP71B130*, and 5′-CCAATGGCTCTAGATGCCCG-3′ (forward) and 5′-GTTTTAATGATGATGATGATGATGTGCAAACAGGTGCTTCTTTG-3′ (reverse) for *CYP71B131a*. Finally, His-tagged CDSs were subcloned into the pYeDP60_GW® expression vector (Dueholm *et al.*, 2015) using the Gateway LR Clonase™ II Enzyme Mix (Invitrogen™, Thermo Fisher Scientific).

Synthesis of CYP71B mutants

Nucleotide sequences of His-tagged *CYP71B* mutants were chemically synthesized and subcloned into the pYeDP60 vector by GenScript Biotech (the Netherlands). Cloning was performed using the Bam*HI* and Eco*RI* restriction enzymes.

Heterologous expression of recombinant CYP71Bs

The pYeDP60 and pYedDP60-GW® vectors containing the various *CYP71Bs* genes, and the empty pYeDP60-GW® as control, were transformed into the WAT21 *Saccharomyces cerevisiae* strain according to Pompon *et al.* (1996) and Urban *et al.* (1997). A single colony from the SGI plates was transferred into 10 ml of SGI liquid medium and incubated at 28°C for 24 h. Subsequently, a 5 ml aliquot of the culture was transferred into 200 ml of YPGE growth medium (Kokina *et al.*, 2014), supplemented with 30 mg l^{-1} adenine, and incubated for an additional 24 h at 28°C. P450 expression was then induced by adding galactose (20 g l^{-1} of growth medium). The induction was carried out for 18 h at 18°C. Microsomal fractions containing heterologous P450s and P450 reductase *At*CPR2 were collected as described in Larbat *et al.* (2007). P450 expression was assessed by western blot, using 6xhistidine Epitope Tag antibodies (Acris, OriGene Technologies, Rockville, MD, USA, Fig. S3).

In vitro characterization of CYP71Bs

A functional screening was performed on CYP71B129, CYP71B130, CYP71B131a and associated mutant enzymes. A total of 77 putative phenolic substrates were tested, including phenylpropenes, coumarins, furanocoumarins and pyranocoumarins (Table S1). For this, microsomal fractions were incubated at 28°C for 30 min in the presence of 200 µM substrate and 200 µM NADPH, in a final volume of 200 µl phosphate buffer, pH 7. Reactions were stopped by the addition of 65 µl acetonitrile : HCL 50 : 50 (1 N). Reaction products were extracted twice with ethyl acetate, air dried, and resuspended in 100 µl methanol : water (80 : 20) for subsequent mass spectrometry analysis. Optimal pH and temperature were determined for CYP71B129, CYP71B130 and CYP71B131a; Km_{app} were determined for all enzymes and mutants using CYP71B130 and CYP71B131a optimal conditions, as described in Villard *et al.* (2021). For the determination of the affinity constant, curves were fitted with the model of Michaelis Menten: $v = V_{max}[S]KM + [S]$.

Identification and quantification of reaction products by mass spectrometry

Reaction products were analyzed using a UHPLC–MS system (Shimadzu, Japan). The elution solvents consisted of ultrapure water with 0.1% formic acid (A) and methanol with 0.1% formic acid (B). The mobile gradient phase was as follows (A/B; v/v): 10 : 90 at 0 min, 60 : 40 at 20 min, 65 : 35 at 32 min, 90 : 10 between 36 and 38.5, and 10 : 90 from 38.51 to 40 min. Compounds were detected based on UV scans and were identified by comparing their retention time and *m/z* ratio to those of standard molecules, and quantified based on 320 nm UV signal, using the LABSOLUTION software (Shimadzu, Japan). Product identity was further confirmed using a UHPLC-HRMS system composed by a Thermo Vanquish liquid chromatographic system (Thermo Scientific) coupled to a tandem mass spectrometer (Orbitrap-IDX; Thermo Scientific). Data were recorded and analyzed on the XCALIBUR™ software (v.2.1.SP1. Build1160; Thermo Fisher Scientific).

Phylogenetic analysis of Moraceous CYP71Bs

A CYP71B dataset (Table S3a) was constituted by performing a similarity search in the genomes and transcriptomic databases of 24 plant species from the nitrogen-fixing clade, available at GenBank (Benson *et al.*, 2012). Genetic resources were screened through BLASTN search using *F. carica* CYP71B131a as query and an e-value of 1000. Full-length putative P450 sequences were isolated, introns were removed, and putative pseudogenes were processed as explained earlier. Most sequences closer to *F. carica* CYP71AS33 than to *F. carica* CYP71B131a were removed. Putative genes received a standardized name from the P450 nomenclature committee (Table S2a). Previously characterized CYP71Bs (Schuhegger *et al.*, 2006; Irmisch *et al.*, 2014; Hansen *et al.*, 2018) and a few representative CYP71ASs were added to the dataset. *Ficus carica* CYP71AH65 was added to constitute the outgroup of the following tree. Nucleotide sequences were aligned with GENEIOUS (Geneious prime 2019, Fig. S4), partitioned on MESQUITE v.3.6 (http://www.mesquiteproject.org) and used to build a Bayesian inference gene-family tree with MRBAYES v.3.2.7 (Ronquist & Huelsenbeck, 2003; Ronquist *et al.*, 2012), as described in Villard *et al.* (2021). This first CYP71B gene tree (Fig. S5) was used to reduce the initial CYP71B dataset to a smaller subset of Moraceae-specific sequences (Table S3a) that were realigned (Fig. S5) and used to generate a second tree, as described above. The trees were drawn with FIGTREE v.1.4.4. Posterior probabilities supporting tree branches were considered weak below 0.7, strong above 0.9.

Comparison of 5-hydroxyxanthotoxin synthases and closely related enzymes

A P450 dataset was assembled using the protein sequences of the eight 5OHXS enzymes described so far (i.e. CYP71B130;

CYP71B131a; CYP71AZ1 (GenBank EF127863.1); CYP71AZ6 (GenBank MH000221.1); CYP82C2 (Genbank NM_119348.2); CYP82C4 (GenBank: NM_119345.3); CYP82D64v1 (*C. clementina* v0.9 genome clementine0.9_007296m); CYP82D64v2 (*C. sinensis* DHSO v3.0 genome Cs_ont_1g009220.1) and seven closely related enzymes which do not display this activity) (i.e. CYP71B129; CYP71AZ3 (GenBank MH000218.1); CYP71AZ4 (GenBank MH000219.1); CYP71AZ5 (GenBank MH000220.1); CYP82C3, (GenBank NM_119346.3); CYP82D92 (Phytozome ID Ciclev10000846m); CYP82D179, (Phytozome ID Ciclev10000844m)). Protein sequences were aligned (Fig. S6) with MAAFT v.7 (https://mafft.cbrc.jp/alignment/server/) relying on default parameters (Kuraku *et al.*, 2013; Katoh *et al.*, 2019), and analyzed on MESQUITE v.3.6 (http://www.mesquiteproject.org).

In silico modeling and docking experiments

CYP71B131a three-dimensional (3D) structures was folded using the COLABFOLD v.1.5.2: ALPHAFOLD2 (Mirdita *et al.*, 2022), using mmseqs2_uniref_env and unpaired-paired MSA options, with standard options for monomeric structure predictions. To model the enzyme–substrate interactions, docking experiments were performed. First, a heme was docked into CYP71B131a 3D-structure. For this, CYP76AH1/miltiradiene (PDB ID: 7cb9) from *Salvia miltiorrhiza* (Gu *et al.*, 2019), was used as a reference and overlapped with CYP71B131a 3D-structure to define a 18 Å × 18 Å × 18 Å docking grid-box around the heme. Protein and heme files were prepared by adding polar hydrogens. A '+2' charge was also added to the heme iron. Rigid docking of the heme (i.e. not allowing the protein to move) was performed using AUTODOCK VINA v.1.2.3 (Trott & Olson, 2010). Subsequently, xanthotoxin and umbelliferone substrates were docked into the CYP71B131a-heme complex. The human microsomal P450 2A6 crystal structure (PDB ID: 1z11) was used as a reference (Yano *et al.*, 2005), and overlapped with the CYP71B131a-heme complex to define a grid-box of 28 Å × 24 Å × 24 Å around the xanthotoxin. Protein file was prepared by adding polar hydrogens, and a '+2' charge was added to the heme iron. Residues within 5Å of xanthotoxin in the reference structure were identified as flexible docking residues. The ligand file was prepared by building bonds and adding polar hydrogen atoms. Flexible docking of the xanthotoxin or the umbelliferone was performed using AUTODOCK VINA v.1.2.3 (Trott & Olson, 2010). CYP71B131a_G373A and CYP71B131a-G373S mutant enzymes were folded and substrates were docked as described above. Visualizations of the docking poses were prepared with PYMOL (DeLano, 2002).

Results

Ficus-Morus CYPome comparison highlights a CYP71B expansion

Since the furanocoumarin pathway appeared multiple times in higher plants, it is not advised to rely on classic similarity search to pursue its elucidation (Villard *et al.*, 2021). Instead, to identify new enzymes involved in furanocoumarin biosynthesis, we relied on lineage-specific evolutionary patterns. In previous work, we demonstrated that the marmesin synthase activity (Fig. 1) emerged relatively recently in the Moraceae, through a CYP76F expansion that occurred after the divergence of the *Ficus* and *Morus* ancestors (Villard *et al.*, 2021). Therefore, we hypothesized that other *Ficus* enzymes catalyzing downstream furanocoumarin-biosynthetic reactions might have similar origins. This means other gene expansions that occurred after the *Ficus-Morus* divergence might enclose other furanocoumarin-biosynthetic enzymes. As target enzymes, we focused on P450s from the CYP71 clan, which play a central role in plant specialized metabolism (Nelson & Werck-Reichhart, 2011) and include all furanocoumarin-related P450s described so far (Fig. 1). Our approach therefore consisted in comparing the CYP71 clan in *F. carica* and *M. notabilis* to identify *Ficus*-specific expansions.

To identify *F. carica* CYP71 clan sequences, we screened the *F. carica* reference genome (Usai *et al.*, 2020). A total of 133 full-length P450 sequences were isolated, corresponding to 85 genes and 48 pseudogenes (Table S2a). These sequences were classified into 18 families and 35 subfamilies of various sizes (Table S2b). Twelve families comprised a single subfamily or single *F. carica* sequence (e.g. CYP84A). The six other families contained multiple subfamilies, with a maximum of 37 *F. carica* CYP71s distributed in eight subfamilies (Table S2b). Interestingly, most multi-sequence subfamilies result from tandem duplications and form physical gene clusters in *F. carica* genome. For instance, all nine *F. carica* CYP71Bs were clustered on *a* ≈ 115 kb fragment of chromosome 11 (Table S2a). *Ficus carica* P450s were then compared to the 97 *M. notabilis* CYP71 clan sequences, previously reported by Ma *et al.* (2014). Even though more sequences were identified in *F. carica* (133) than *M. notabilis* (97), all 35 subfamilies observed in *F. carica* were present in *M. notabilis*, and six additional single-sequence subfamilies were only observed in *M. notabilis* (Table S2b).

Ficus carica and *Morus notabilis* CYP71 clan sequences were then used to generate a protein-family phylogenetic tree (Fig. 2). Across this phylogeny, some families and subfamilies were highly conserved. For example, the CYP78A subfamily comprises six *F. carica* and *M. notabilis* pairs of orthologs, meaning that the last common *Ficus-Morus* ancestor likely possessed six CYP78As. This analysis also revealed significant lineage-specific expansions of the CYP71B, CYP71AN, and CYP76F subfamilies in *F. carica*, and of the CYP82D subfamily in *M. notabilis* (Fig. 2). Since the CYP76F diversification gave rise to the marmesin synthase activity (Villard *et al.*, 2021), we assumed the CYP71B and CYP71AN expansions might have given rise to other furanocoumarin-biosynthetic enzymes. Among these two subfamilies, the most drastic expansion occurred in the CYP71Bs, with one single *M. notabilis* sequence compared to nine *F. carica* orthologs (CYP71B129, CYP71B130, CYP71B131a, CYP71B131b, CYP71B133, CYP71B134, CYP71B135, CYP71B136, CYP71B137, Fig. 2). We therefore decided to focus on *F. carica* CYP71Bs for further characterization.

New Phytologist

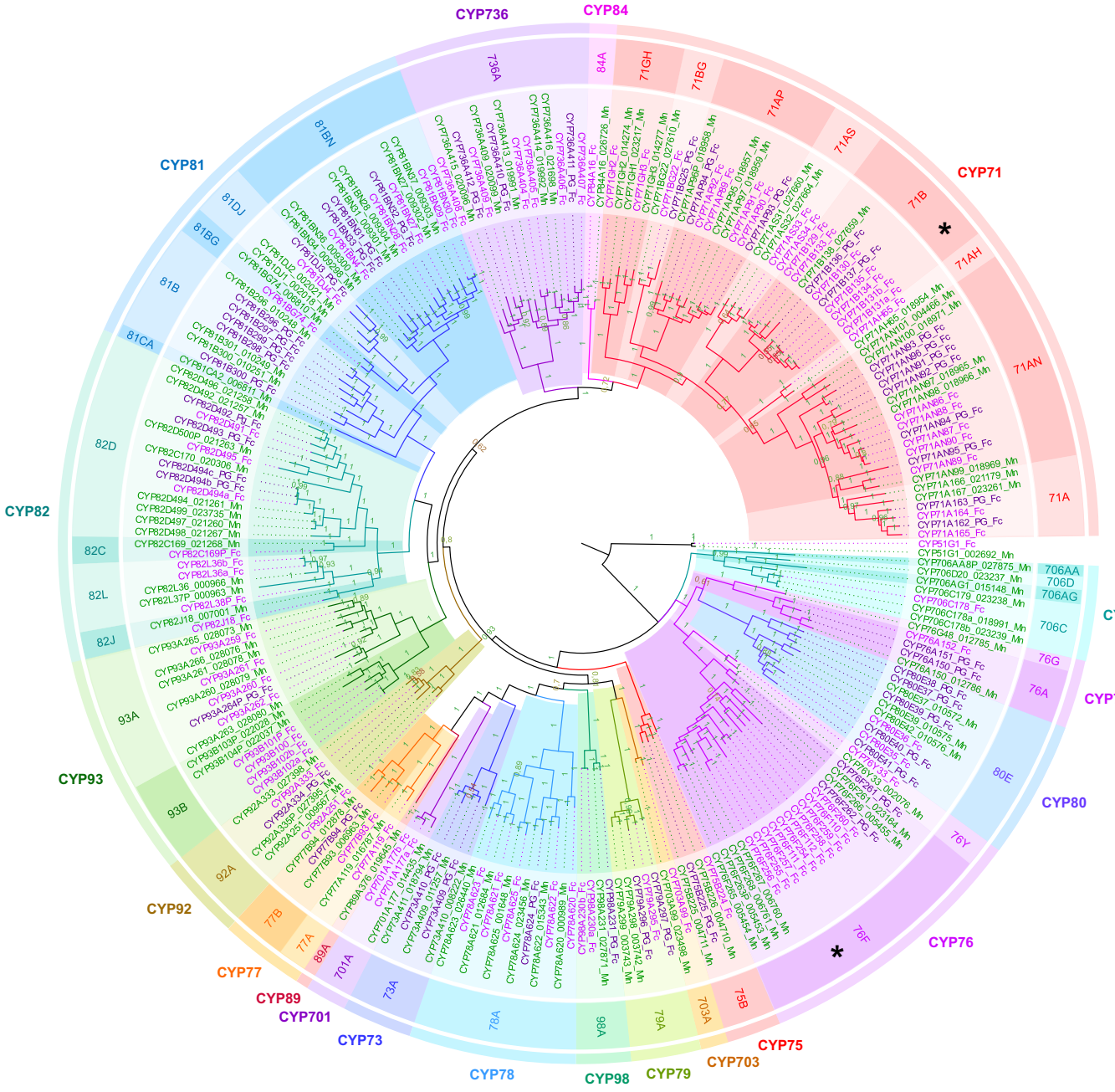

Fig. 2 Comparison of the CYP71 clan in *Ficus carica* and *Morus notabilis*. Bayesian inference tree of *Ficus carica* and *M. notabilis* CYP71 clan, rooted on the CYP51 clan. *Ficus carica* genes are colored in light purple, *F. carica* pseudogenes in dark purple, *M. notabilis* genes in green. Scale bar = 0.09 For an easier understanding of the tree, clades are colored by P450 (sub)families, P450 (sub)family names are detailed, and the CYP76F and CYP71B subfamilies are highlighted with a black asterisk. *Morus notabilis* sequence names include the accession numbers given in Ma *et al*. (2014). Branch labels indicate posterior probabilities, branch length indicates the number of substitutions per site.

CYP71Bs include two 5-hydroxyxanthotoxin synthases (5OHXS) and one umbelliferone hydroxylase

To investigate the function of the nine *F. carica* CYP71Bs, we cloned them from *F. carica* leaf RNA. Three genes were successfully amplified: *CYP71B129*, *CYP71B130* and *CYP71B131a*. CYP71B129–131a enzymes were heterologously produced in yeast (Fig. S3) and used to perform *in vitro* enzyme assays in the presence of NADPH and 77 putative substrates belonging to the coumarin, furanocoumarin, pyranocoumarin and phenylpropene families (Table S1). Results demonstrated that CYP71B130 and CYP71B131a were both able to convert xanthotoxin into 5-hydroxyxanthotoxin, making them 5OHXS enzymes (Figs 3, S7). The identity of the product was formally identified by comparing its mass spectrometry characteristics to a commercial 5-hydroxyxanthotoxin standard.

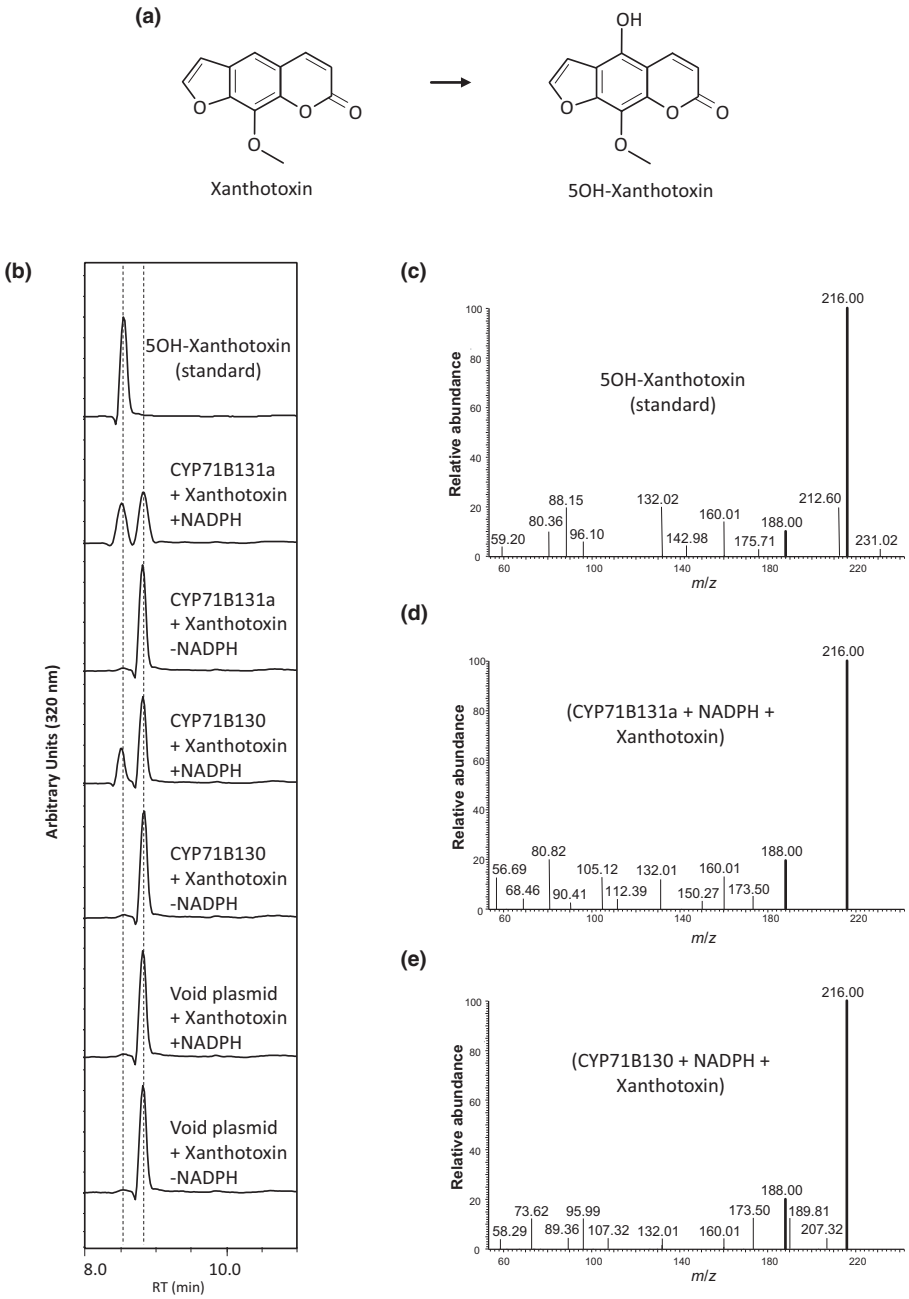

Fig. 3 Conversion of xanthotoxin into 5-hydroxyxanthotoxin by CYP71B130 and CYP71B131a. (a) Molecular representation of the reaction. (b) High-performance liquid chromatography (HPLC) separation profiles. CYP71B130, CYP71B131a, and empty plasmid (Ø plasmid) were incubated with xanthotoxin, in the presence and absence of nicotinamide adenine dinucleotide phosphate (NADPH). (c–f) Tandem mass spectrometry fragmentation patterns of (c) the standard 5-hydroxyxanthotoxin, (d) and (e) the reaction product obtained with CYP71B131a and CYP71B130, respectively.

By contrast, CYP71B129 did not metabolize any of the tested furanocoumarins, but hydroxylated the coumarin umbelliferone (UMBH activity, Fig. 4). Theoretically, umbelliferone can be hydroxylated on five different carbons, leading to the production of 3,7-, 4,7-, 5,7-, 6,7- or 7,8- dihydroxycoumarin. Out of these five molecules, only four standards are commercially available, *that is* 4,7-, 5,7-, 6,7- and 7,8- dihydroxycoumarin. Using mass spectrometry (Fig. S7), we compared these four standards to CYP71B129 reaction product, showing that only 7,8-dihydroxycoumarin (daphnetin) had the same retention time as the product. This indicates that CYP71B129 produces either daphnetin or the untested 3,7-dihydroxycoumarin. As the amount of product synthesized by CYP71B129 was too low to consider an NMR investigation, we could not further confirm where the hydroxylation was performed.

Next, further enzymatic characterization showed that optimal activities of the three enzymes CYP71B129-131a with their respective substrates were obtained at pH 7.3–7.9 and a temperature of 24–26°C (Figs S8, S9). The apparent *Km* values associated with these enzymes were also determined, showing that CYP71B130 (Km_{app} of 0.9 ± 0.7 μM) has a 10-times higher affinity for xanthotoxin than CYP71B131a (Km_{app} of 9.4 ± 1.2 μM) (Fig. S10a,b). The Km_{app} associated with umbelliferone hydroxylation by CYP71B129 was 28.5 ± 9.3 μM (Fig. S10d).

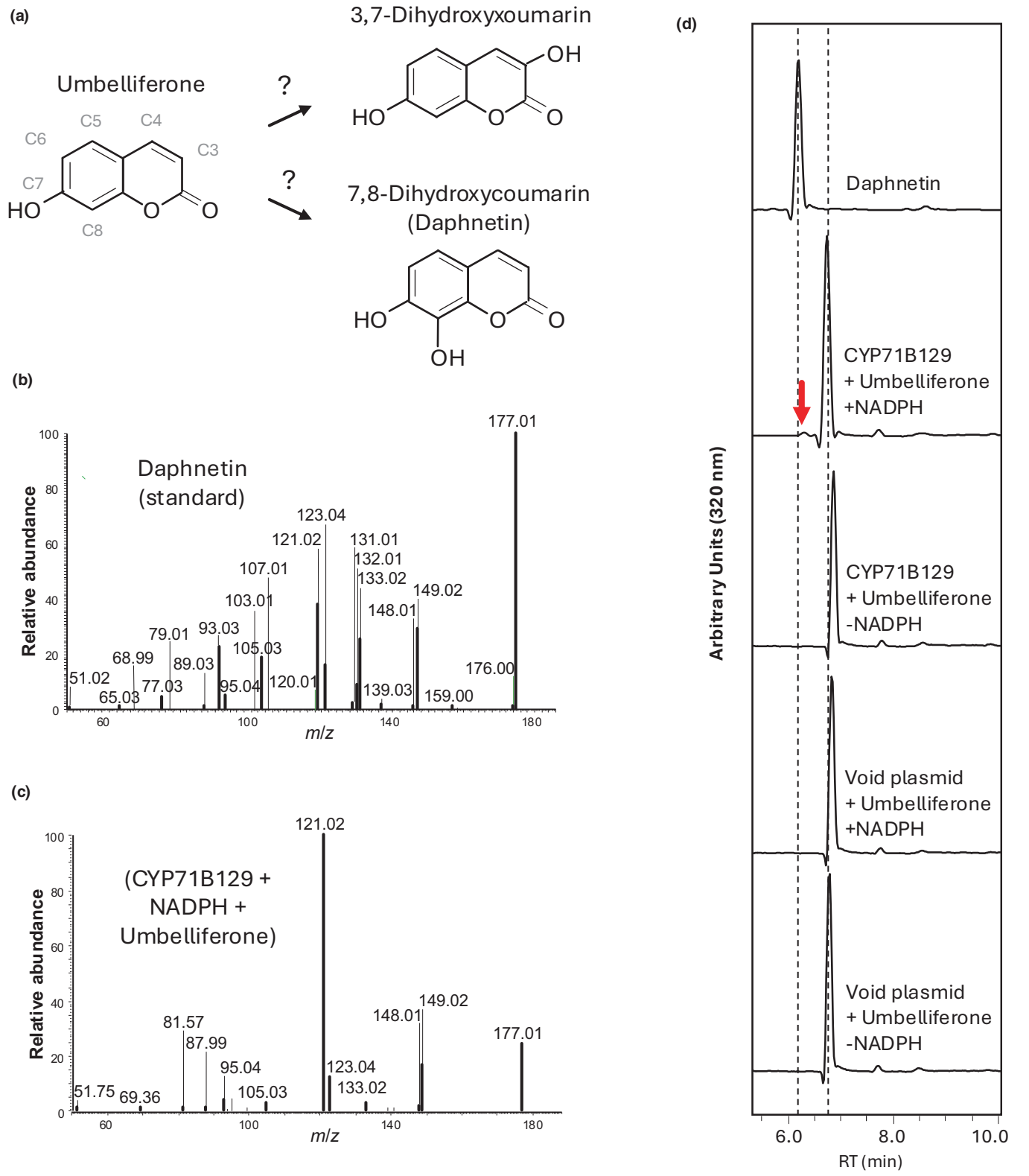

Fig. 4 Metabolization of umbelliferone by CYP71B129. (a) Molecular representation of the reaction. Carbon numbering is indicated on the molecule. Tandem mass spectrometry fragmentation patterns of (b) daphnetin standard and (c) the reaction product with CYP71B129. (d) High-performance liquid chromatography (HPLC) separation profiles with CYP71B129 and the empty plasmid (Ø plasmid) incubated with daphnetin, in the presence and absence of nicotinamide adenine dinucleotide phosphate (NADPH). The red arrow indicates the product of the reaction.

The 5-hydroxyxanthotoxin synthase activity emerged in subclade B3 of Moraceous CYP71Bs

CYP71B129–131a are three *F. carica* enzymes sharing 83–88% nucleotide identity. However, CYP71B129 metabolizes a coumarin, while CYP71B130 and CYP71B131a metabolize a furanocoumarin. To better understand the evolution of these enzymes, we performed a gene phylogenetic analysis. Screening 24 plant genomes, we identified 82 CYP71B sequences corresponding to 58 genes and 24 pseudogenes (Table S3a). Sequences were used to generate a gene-family phylogenetic tree (Fig. S5). On this gene-tree, all Rosales CYP71Bs form a well-supported clade which topology perfectly reflects the Rosales phylogeny (Zuntini *et al.*, 2024). This indicates that the last common Rosales ancestor possessed a single CYP71B sequence, which either remained low-copy (e.g. Rosaceae family) or diversified in a lineage-specific manner (e.g. Moraceae family, Fig. S5).

Zooming on the gene-tree (Fig. 5a), we focused on Moraceae-specific CYP71Bs and classified them into two clades (A–B) comprising a total of four subclades (A, B1-B3). Clade A consists of all *Morus* and *Artocarpus* CYP71Bs. These CYP71Bs are well-conserved and present as single- or low-copy in the five screened *Morus* and *Artocarpus* genomes (Fig. 5a). Contrarily, clade B comprises all *Ficus* and *Antiaris* CYP71Bs. Each screened *Ficus* and *Antiaris* genome contained 4–14 CYP71B sequences, indicating significant expansion. Clade B is further subdivided into subclades B1-B3: each of these subclades contains both *Ficus* and *Antiaris* sequences, and therefore, predates the divergence of the *Ficus* and *Antiaris* ancestors (Fig. 5a,b). *Ficus carica* CYP71B129 belongs to subclade B2, CYP71B130 and CYP71B131a to subclade B3. The relatively low expansion and short branch-lengths observed in subclade B2 suggest that the CYP71B129 UMBH activity might not be a B2-specific novelty. Instead, it may be shared with clade A and subclade B1. Additional experiments are, however, required to support this hypothesis. Contrarily, sequences from subclade B3 diversified and accumulated more mutations, suggesting the 5OHXS activity observed in *F. carica* CYP71B130 and CYP71B131a emerged in this subclade. This means all B3-enzymes might be 5OHXSs.

To further investigate the emergence of 5OHXS activity within the CYP71Bs, we used our sequence alignment (Fig. S11) to compare the substrate recognition sites (SRSs, Table S3b) throughout the CYP71B phylogeny (Gotoh, 1992). Results highlighted seven SRS-residues (Fig. 5a) that were well-conserved in subclades A-, B1, and B2 (L116, Q211, A313, V318, P312, A373, T492, numbered according to CYP71B131a equivalents) but substituted in all B3-sequences (V116, H211, S313, I318, A372, G373, S492). These B3-specific synapomorphies might have played a key role in the emergence of 5OHXS activity. Remarkably, SRS-residues were relatively well-conserved throughout the B3 subclade, suggesting that even early branching B3-genes likely encode 5OHXSs (i.e. *CYP71B135s*, *CYP71B164s*). For instance, only nine SRS-residues were different between the two characterized 5OHXS, that is H/Q104, K/R108, L/Q114, H/R248, Q/E249, I/V315, G/A320, L/I481 and A/T487 in CYP71B130/131a, respectively. These mutations probably explain the activity difference measured between the two enzymes. Among them, H104, K108, L115, Q248 and G320 are unique in subclade B3, as they are only observed in the six CYP71B130 sequences (Fig. 5a). These five recent mutations might thus be responsible for an increased 5OHXS activity in CYP71B130s.

Taken together, our results indicate that the 5OHXS activity emerged in subclade B3 of Moraceous CYP71Bs, probably from the UMBH activity. This evolution correlates with a few mutations affecting the SRSs. The 5OHXS activity therefore results from a lineage-specific CYP71B-diversification that happened after the divergence of the Ficeae and Moreae tribes, but before the divergence of the Ficeae and Olmedieae tribes. This pattern is consistent with the repartition of known furanocoumarin-producing species of the Moraceae family (Fig. 5b).

5-hydroxyxanthotoxin synthases possess a glycine in position 373

If the 5OHXS function emerged recently in the CYP71Bs, it has also been described in other P450 subfamilies, that is CYP71AZ, CYP71B, CYP82C and CYP82D (Kruse *et al.*, 2008; Krieger *et al.*, 2018; Limones-Mendez *et al.*, 2020). To understand 5OHXS independent emergence in distant P450 subfamilies, we compared the eight characterized 5OHXS enzymes (i.e. CYP71AZ1, CYP71AZ6, CYP71B130, CYP71B131a, CYP82C2, CYP82C4, CYP82D64v1, CYP82D64v2) with seven closely related enzymes which do not exhibit this activity (i.e. CYP71AZ3, CYP71AZ4, CYP71AZ5, CYP71B129, CYP82C3, CYP82D92, CYP82D179). For this, we aligned the protein sequences of the different enzymes and analyzed the SRSs throughout the alignment (Fig. S11). Overall, SRS-residues were either well-conserved across all sequences, varied according to P450 families or subfamilies, or varied without a clear pattern (Table 1; Fig. S11). However, out of the 96 SRS-residues, residue 373 displayed a unique pattern (Table 1; Fig. S11). Indeed, all investigated 5OHXS enzymes possessed a glycine in position 373 while non-5OHXS enzymes possessed either an alanine (CYP71B129, CYP71AZ3, CYP71AZ5, CYP82C3), a valine (CYP82D92) or a serine (CYP82D179). The only non-5OHXS enzyme possessing a glycine at this position was CYP71AZ4, which catalyzes another furanocoumarin-biosynthetic reaction (i.e. xanthotoxol synthase) (Krieger *et al.*, 2018). Additionally, G373 was also one of the seven B3-specific amino acids highlighted above (Fig. 5a). This unique and intriguing pattern hinted toward a critical role of residue 373 for the 5OHXS activity.

To explore this further, we docked the xanthotoxin substrate into CYP71B131a 3D-model (Fig. 6a) and defined the enzyme's catalytic pocket as the 27 residues located at less than 5 Å from the substrate (Table 1). These 27 residues form a subgroup of the 96 SRS-residues. Interestingly, residue 373 was included in this catalytic pocket, in very close proximity (≃3 Å) to xanthotoxin's furan ring (Fig. 6d).

New Phytologist

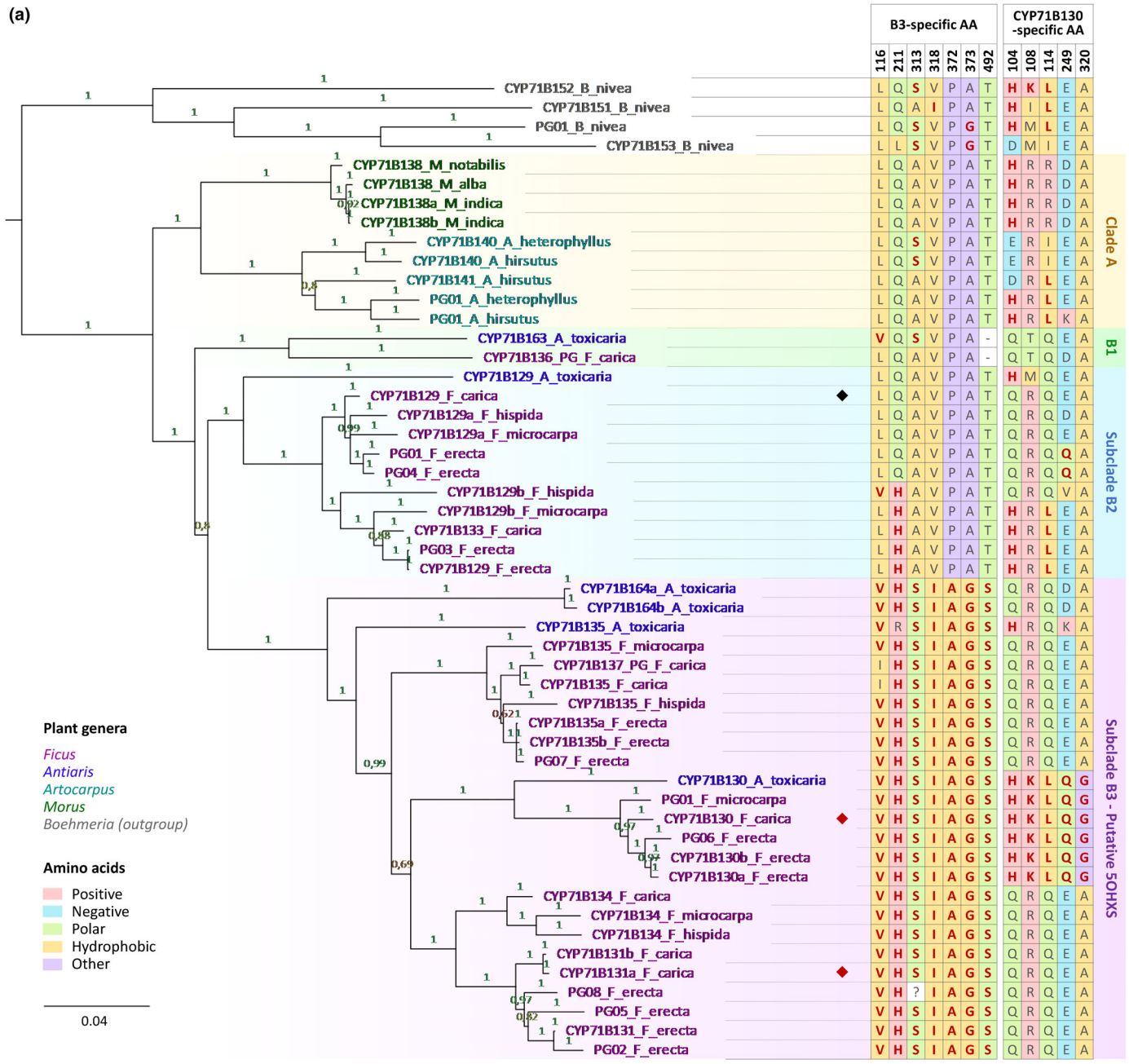

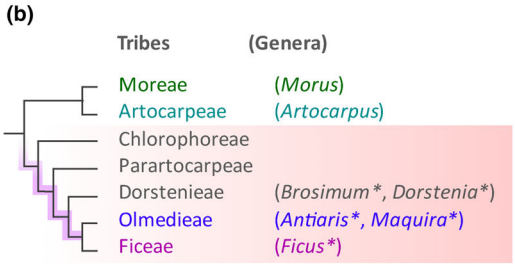

Fig. 5 Emergence of the 5OHXS activity in the Moraceae family. (a) Gene-family tree of the CYP71Bs from the Moraceae family, rooted on CYP71Bs from *Boehmeria nivea* (Urticaceae). Characterized 5-hydroxyxanthotoxin synthase (5OHXS) are highlighted with a red diamond, characterized umbelliferone hydroxylase (UMBH) with a black diamond. Amino acids (AAs) of interest from the Substrate Recognition Sites (SRSs) are reported through the phylogeny, numbered according to *Ficus carica* CYP71B131a equivalent. Amino acids corresponding to CYP71B130 derived character states are highlighted in bold red, others are in gray. Branch labels indicate posterior probabilities, branch length indicates the number of substitutions per site. (b) Phylogeny of the Moraceae family, adapted from (Gardner *et al*., 2021). The tribes containing known furanocoumarin-producing genera (*Ficus*, *Antiaris*, *Maquira*, *Brosimum* and *Dorstenia*) are highlighted in red (Rovinski *et al*., 1987; Vieira *et al*., 1999; Abegaz *et al*., 2004; Shi *et al*., 2014; Takahashi *et al*., 2017). The putative emergence of the 5OHXS activity in Moraceous CYP71Bs is highlighted in purple.

Residue 373 strongly impacts CYP71B131a enzymatic activity

To experimentally investigate the impact of amino acid 373 on the 5OHXS enzyme activity, we designed a series of CYP71B131a mutants, in which G373 was substituted with an alanine (A), serine (S) or valine (V). These substitutions correspond to the amino acids observed in the non-5OHXS P450 enzymes described above. Each substitution introduces a gradual steric hindrance (G < A < S < V) and/or variable polarity (S) (Table 2). CYP71B131a mutant genes were synthesized, and associated enzymes were expressed and characterized. Results showed that CYP71B131a_G373A and CYP71B131a_G373S could still catalyze the 5OHXS reaction (Figs S11, S12). The affinity of CYP71B131a_G373A for xanthotoxin was 3-times lower than that of the wild-type enzyme (Km_{app} = 20.8 ± 8 μM). The activity of CYP71B131a_G373S was too low to accurately determine its Km_{app}. For CYP71B131a_G373V, no 5OHXS activity was detected. The three mutant enzymes were also incubated in the presence of umbelliferone. Interestingly, they all exhibited the UMBH activity (Figs S10, S12), and showed a rather high affinity for umbelliferone (Km_{app} = 9.3 ± 8.9 μM for CYP71B131a_G373A; 12.3 ± 9.9 μM for CYP71B131a-G373S, Fig. S10e,f). Next, to test if a glycine in position 373 would be enough to recover the 5OHXS activity, we designed a CYP71B129_A373G mutant and characterized the associated enzyme. No 5OHXS activity was detected, and CYP71B129_A373G still exhibited traces of UMBH activity (Figs S12, S13h).

To understand the impact of the G373A and G373S mutations on CYP71B131a 5OHXS activity, we built 3D-models of the associated mutant enzymes and performed docking experiments with xanthotoxin and umbelliferone. Xanthotoxin dockings showed that substituting G373 by an alanine or a serine slightly pushes the xanthotoxin and modifies its orientation toward the heme (Fig. 6e). Given the experimental results, this altered position might not be favorable for xanthotoxin binding. In the case of umbelliferone, amino acid 373 had an even stronger impact. Indeed, the best docking state obtained with CYP71B131a positioned umbelliferone with its carbons C4 and C5 oriented toward the heme iron. By contrast, docking performed with CYP71B131a_G373A and CYP71B131a_G373S resulted in a horizontal rotation of umbelliferone, positioning carbon C8 toward the heme iron (Fig. 6c). These results strongly suggest that CYP71Bs' UMBH activity corresponds to a C8 hydroxylation, and thus, to daphnetin production. This would also explain why the wild-type CYP71B131a does not exhibit this activity.

In summary, our results demonstrated that amino acid 373 plays an important role in shaping the CYP71B131a active site and directly impacts substrate specificity and affinity. Indeed, increased steric hindrance at position 373 influences the positioning of the substrate in the active site, resulting in a decreased affinity for xanthotoxin and an increased affinity for umbelliferone. However important, amino acid 373 was not critical for the acquisition of the 5OHXS function in CYP71Bs, as CYP71B131a_G373A still exhibited 5OHXS activity while CYP71B129_A373G did not. This suggests additional residues must also play an essential role in the 5OHXS activity.

Discussion

PSMs are molecules of ecological and societal interest with applications in medicine, agronomy, cosmetics, and in the agri-food industry (Weng *et al*., 2021). As plants do not usually produce enough PSMs quantities to cover large-scale applications, a major challenge of the field consists in elucidating PSM biosynthetic pathways, to help to develop biotechnological tools for large-scale production (Ono & Murata, 2023). This also provides new insights into plant biochemistry and can help better understand PSM ecological roles.

In this study, we developed a strategy leveraging well-established phylogenetic tools to identify enzymes involved in the biosynthesis of lineage-specific PSMs, and we applied it to furanocoumarin biosynthesis. For this, we compared the genes of two Moraceae with different PSM profiles: *F. carica* and *M. notabilis*. As far as we know, furanocoumarins are indeed present in *Ficus* but not in *Morus*, and likely appeared in Moraceae after the *Ficus-Morus* divergence (Villard *et al*., 2021). To identify furanocoumarin-biosynthetic-specific genes, we thus looked for lineage-specific gene expansions which could correlate with furanocoumarin lineage-specific emergence. This led to the identification of a CYP71B diversification, amongst which two enzymes exhibited the 5OHXS activity. Our approach therefore proved successful and could be generalized to other families of PSMs, enzymes, and plants, provided that the target PSM is lineage-specific and its repartition in plants is known. If phylogenetics is widely used to analyze characterized-enzymes and look for orthologs, it has so far rarely been used to select candidate enzymes with a potential new function, and only as a minor tool

New Phytologist (2025)
www.newphytologist.com

Table 1 Residues belonging to the substrate recognition sites (SRSs) and positioned close to the substrate (5 Å) in 5-hydroxyxanthotoxin synthases (5OHXSs) and non-5OHXSs P450 enzymes.

SRS		1											2		3	4							5					6
Residues		104	106	111	114	115	116	117	118	120	121	122	213	217	247	303	304	305	307	308	309	312	372	373	376	377	379	491
5OHXS	CYP71B130	H	**A**	**Y**	**L**	**D**	**V**	**A**	**F**	**P**	**Y**	**G**	**A**	**M**	**F**	**L**	**N**	**M**	**L**	**G**	**G**	**T**	**A**	**G**	**L**	**L**	**R**	**L**
	CYP71B131a	**Q**	**A**	**Y**	Q	**D**	**V**	**A**	**F**	**P**	**Y**	**G**	**A**	**M**	**F**	**L**	**N**	**M**	**L**	**G**	**G**	**T**	**A**	**G**	**L**	**L**	**R**	**L**
	CYP71AZ1	T	M	**Y**	**L**	**D**	**V**	**A**	**F**	**P**	**Y**	S	L	L	**F**	**L**	**N**	V	N	**G**	**G**	**T**	T	**G**	**L**	I	**R**	**I**
	CYP71AZ6	T	M	**Y**	**L**	**D**	**V**	**A**	**F**	T	**Y**	S	I	L	**F**	**L**	**N**	V	N	**G**	**G**	**T**	T	**G**	**L**	I	**R**	**L**
	CYP82D64v1	V	G	**Y**	S	L	L	G	**F**	**P**	**Y**	**G**	F	**M**	A	**L**	A	L	**L**	**G**	**G**	**T**	**A**	**G**	**L**	A	**R**	**L**
	CYP82D64v2	V	G	**Y**	S	L	L	G	**F**	**P**	**Y**	**G**	F	**M**	A	**L**	A	L	**L**	**G**	**G**	**T**	**A**	**G**	**L**	A	**R**	**L**
	CYP82C2	A	**A**	**Y**	A	V	F	G	**F**	**P**	**Y**	S	F	V	G	**L**	A	L	**L**	**G**	**G**	**T**	**A**	**G**	**L**	G	**R**	**L**
	CYP82C4	A	**A**	**Y**	A	V	F	G	**F**	**P**	**Y**	S	F	I	G	**L**	A	L	**L**	**G**	**G**	**T**	**A**	**G**	**L**	G	**R**	**L**
Non-5OHXS	CYP71B129	**Q**	**A**	**Y**	Q	**D**	L	**A**	**F**	**P**	**Y**	**G**	**A**	**M**	**F**	**L**	**N**	**M**	**L**	**G**	**G**	**T**	P	A	**L**	**L**	**R**	**L**
	CYP71AZ3	T	M	**Y**	**L**	**D**	**V**	**A**	**F**	**P**	**Y**	T	I	F	**F**	**L**	**N**	V	N	**G**	**G**	**T**	P	A	**L**	V	**R**	**L**
	CYP71AZ4	T	S	**Y**	**L**	E	M	**A**	**F**	**P**	**Y**	**G**	I	F	**F**	**L**	**N**	V	S	**G**	**G**	**T**	P	**G**	**L**	I	**R**	**L**
	CYP71AZ5	T	T	**Y**	**L**	**D**	M	**A**	**F**	**P**	**Y**	S	L	S	**F**	Q	**N**	I	N	**G**	**G**	**T**	P	A	**L**	**L**	**R**	–
	CYP82D92	L	M	**Y**	S	M	F	G	**F**	**P**	**Y**	**G**	S	S	A	**L**	G	L	**L**	A	A	**T**	**A**	V	**L**	V	H	L
	CYP82D179	L	M	**Y**	S	M	F	G	**F**	**P**	**Y**	**G**	F	S	A	M	G	L	**L**	A	A	N	**A**	S	S	I	H	**L**
	CYP82C3	A	**A**	**Y**	–	–	–	–	–	–	–	–	F	V	R	**L**	A	L	**L**	**G**	**G**	**T**	**A**	A	**L**	G	**R**	**L**

Residues conserved in most investigated sequences are highlighted in light blue, residues with a clear P450 family or subfamily patterns are highlighted in light yellow, residue varying according to P450 function is highlighted in light red, more variable residues are in white. Amino acids identical to the CYP71B131a equivalents are in bold red, others are in black. Residues are numbered according to the CYP71B131a equivalent.

New Phytologist

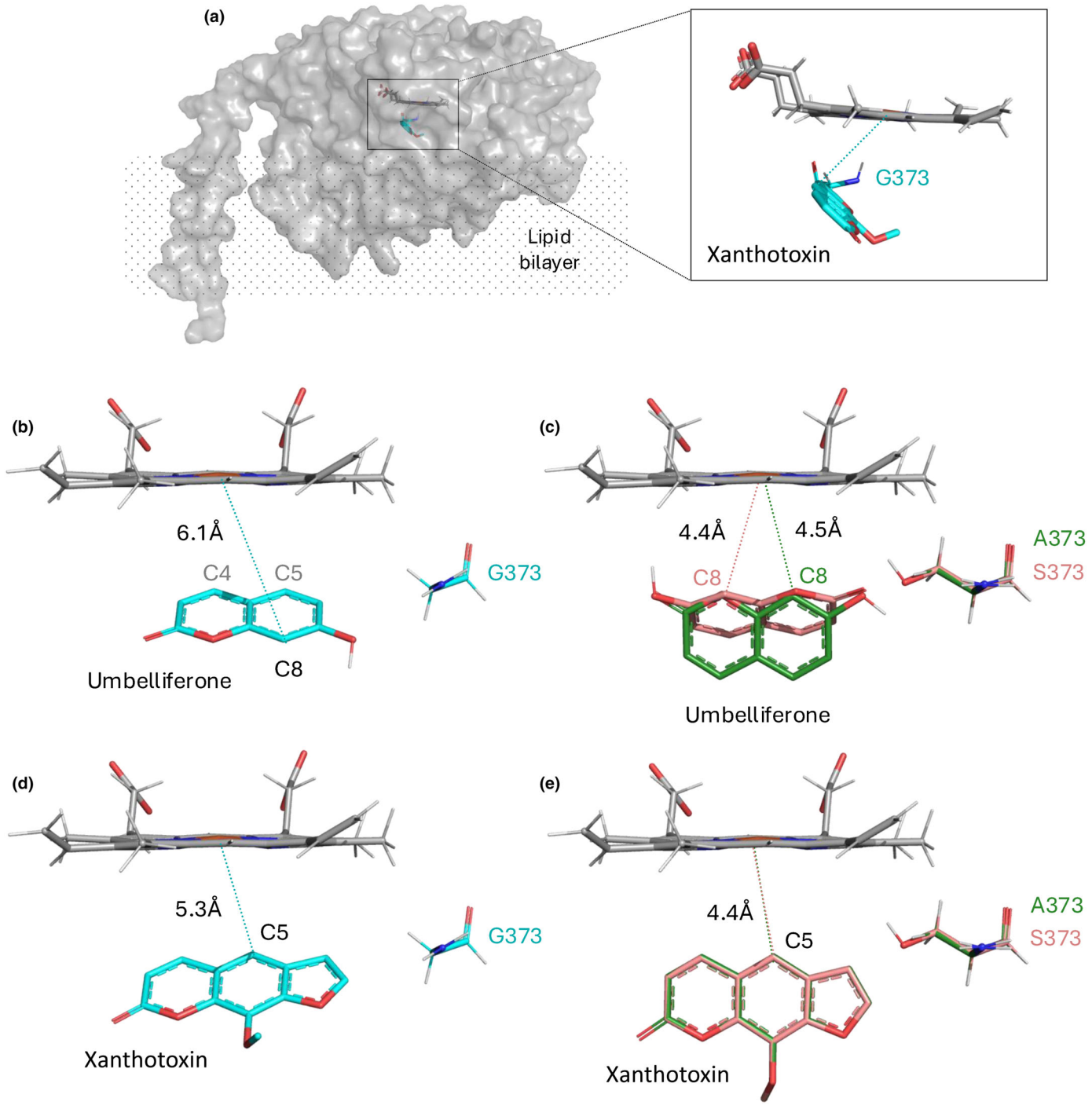

Fig. 6 Docking of xanthotoxin and umbelliferone into CYP71B131a and associated mutant enzymes. (a) Three-dimensional model of CYP71B131a in complex with a heme (gray) and umbelliferone or xanthotoxin. (b–e) Most probable binding mode of umbelliferone (b, c) and xanthotoxin (d, e) into CYP71B131a (b, d) and associated mutants (c, e). Substrates are colored according to the enzyme they are docked in: blue for CYP71B131a, green for CYP71B131a_G373A, pink for CYP71B131a-G373S. Distance between substrates' carbons and the heme iron are highlighted with dashed lines.

complementing classic approaches (Hodgson *et al.*, 2019; Pluskal *et al.*, 2019). Our proposed approach is therefore original but supported by many examples of lineage-specific enzymes producing lineage-specific PSMs, as reviewed by Pichersky & Lewinsohn (2011). Moreover, as it only requires genomic resources which are now plentiful and easy to generate, it can be applied to virtually any lineage-specific PSM, regardless of previously limiting factors such as convergent evolution and low-PSM production. Our approach therefore has great potential to help address the classic bottlenecks of specialized enzyme discovery. Of course,

Table 2 Overview of the activities of wild-type CYP71Bs and associated mutants.

P450 name	AA 373	Steric hyndrance	Xanthotoxin	Umbelliferone
CYP71B130	**G**	$>CH_2$	+ (0.9 ± 0.7 μM)	–
CYP71B131a	**G**	$>CH_2$	+ (9.4 ± 1.2 μM)	–
CYP71B131a_G373A	A	$>CH\text{-}CH_3$	+ (20.8 ± 8 μM)	+
CYP71B131a_G373S	S	$>CH\text{-}CH_2OH$	+	+
CYP71B131a_G373V	V	$>C\text{-}CH<^{CH_3}_{CH_3}$	–	+
CYP71B129_A373G	G	$>CH_2$	–	+
CYP71B129	**A**	$>CH\text{-}CH_3$	–	+ (28.5 ± 9.3 μM)

Wild-type enzymes are indicated in bold, while mutants are in regular font. The ability of the different enzymes to metabolize or not the xanthotoxin and umbelliferone substrates are indicated with (+) and (–), respectively. When applicable, the apparent *Km* (Km_{app}) were reported (μM). The catalytic parameters are the means of three independent replicates, and errors represent SD.

it also has limits: for instance, it cannot highlight newly functionalized enzymes that evolved without prior major gene duplications. However, evolving new functions without gene duplications is relatively rare (Yu *et al.*, 2015). Our approach thus constitutes an excellent tool to elucidate PSM biosynthesis pathways and can be used in combination with other existing approaches. Finally, it also means that the CYP71AN expansion observed in *F. carica* likely includes enzymes involved in the production of furanocoumarins or another lineage-specific PSM.

Experimental results showed that CYP71B129–131a are highly selective enzymes hydroxylating umbelliferone (CYP71B129) or converting xanthotoxin into 5-hydroxyxanthotoxin (CYP71B130,131a). The affinity of CYP71B130 (Km_{app} = 0.9 ± 0.7 μM) and CYP71B131a (Km_{app} = 9.4 ± 1.2 μM) for xanthotoxin falls within the classic affinity range determined for previously characterized xanthotoxin hydroxylases (i.e. CYP82D64v1, Km_{app} = *4.6* ± 1.7 μM; CYP82D64v2, Km_{app} = 7.4 ± 4.0 μM; CYP71AZ1, Km_{app} = 13.1 ± 3.2 μM) and other furanocoumarin-biosynthetic P450s (i.e. Km_{app} ≈ 0.5–13 μM for CY71AJ1–4, CYP71AZ4,6) (Krieger *et al.*, 2018; Limones-Mendez *et al.*, 2020). The only exception so far is CYP76F112, which displays a very high affinity (Km_{app} = 32.2 ± 3.9 nM) for demethylsuberosin (Villard *et al.*, 2021). On the contrary, P450s involved in coumarin biosynthesis often have lower affinity for their substrate. This is for instance, the case of CYP71AZ3, which displays a rather low affinity (Km_{app} = 248.6 ± 51.9 μM) for esculetin (Krieger *et al.*, 2018). This is also consistent with CYP71B129 slightly lower affinity for umbelliferone (Km_{app} = 28.5 ± 9.3 μM). In addition, according to the Kitajima *et al. Ficus carica* RNA-Seq libraries, *CYP71B130* and *CYP71B131a* are overexpressed in petiole latex (Kitajima *et al.*, 2018), which has a high-furanocoumarin content (Munakata *et al.*, 2020). Taken together, the high selectivity and relatively good affinity of CYP71B129–131a, their expression patterns, and the presence of both umbelliferone and xanthotoxin substrates in *Ficus carica* (Mamoucha *et al.*, 2016), suggest that the UMBH and 5OHXS activities might be CYP71B129 and CYP71B130-131a physiological functions, respectively. However, to the best of our knowledge, associated products were never reported in *Ficus*. This could be because these products are not often included in metabolomic studies, or because they do not accumulate in *Ficus* but are instead quickly converted into different compounds. To confirm CYP71B129–131 *in planta* activity, another possibility consists in knocking-out or overexpressing the associated genes in fig trees and investigating the metabolome of resulting transgenic plants. However, even this approach is not undeniable, as other enzymes could take over.

Furanocoumarins are lineage-specific PSMs which derive from ubiquitous coumarins such as umbelliferone (Fig. 1) (Munakata *et al.*, 2020). Interestingly, several furanocoumarin-biosynthetic enzymes were found to metabolize coumarins and/or to be closely related to coumarin-biosynthetic enzymes (Kruse *et al.*, 2008; Krieger *et al.*, 2018; Rajniak *et al.*, 2018; Limones-Mendez *et al.*, 2020). For instance, within the CYP71AZ subfamily, CYP71AZ3 metabolizes esculetin (coumarin), CYP71AZ4 metabolizes scopoletin (coumarin) and psoralen (furanocoumarin), while CYP71AZ1 and CYP71AZ6 metabolize xanthotoxin (furanocoumarin) (Krieger *et al.*, 2018). In this study, we observed a similar pattern in the CYP71B subfamily, as it includes both UMBH (coumarin) and 5OHXS (furanocoumarin) activities. Moreover, our phylogenetic analyses strongly suggest that CYP71B 5OHXS activity evolved from the UMBH activity, via duplications and functional divergence of the *UMBH* genes. As closely related P450s often metabolize similar compounds (Nelson & Werck-Reichhart, 2011), CYP71B functional divergence was likely facilitated by the structural similarity between umbelliferone and xanthotoxin. The CYP71B subfamily therefore perfectly exemplifies how furanocoumarin-biosynthetic enzymes can stem from coumarin-biosynthetic ones.

In previous studies, CYP71AZ1, CYP71AZ6, CYP82C2, CYP82C4, CYP82D64v1 and CYP82D64v2 were described as 5OHXS enzymes (Kruse *et al.*, 2008; Krieger *et al.*, 2018;

Limones-Mendez *et al.*, 2020). With the characterization of CYP71B130 and CYP71B131a, the 5OHXS activity has now been identified in four P450 subfamilies. To better understand how multiple P450 subfamilies acquired the ability to metabolize xanthotoxin, we decided to perform SRS analyses. The SRSs are small regions of P450 enzymes known to regulate substrate specificity. Hence, amino acid substitutions affecting the SRSs often result in significant activity changes such as substrate range, affinity, regio- and stereoselectivity (Gotoh, 1992; Villard *et al.*, 2021). First, we focused on the CYP71B subfamily and identified seven SRS- amino acids that were well-conserved in most Moraceous CYP71Bs but substituted in all putative 5OHXSs from subclade B3 (i.e. substitutions L116V, Q211H, A313S, V318I, P372A, A373G, T492S). In CYP76F112, similar evolutionary patterns were described for four SRS- amino acids that were experimentally shown to impact substrate specificity and affinity (Villard *et al.*, 2021). It can thus reasonably be assumed that (some of) the seven 5OHXS-specific SRS-substitutions identified in the CYP71Bs played a key role in the substrate specificity switch from umbelliferone to xanthotoxin. Then, we extended our analysis to the CYP71B, CYP71AZ, CYP82C and CYP82D subfamilies and identified an SRS-amino acids displaying a unique pattern: all 5OHXSs from the four subfamilies possessed a glycine in position 373, while non-5OHXS enzymes possessed a different amino acid at this position. Experimental results showed that increased steric hindrance at position 373 lowered CYP71B131a affinity for xanthotoxin and allowed umbelliferone metabolization. These results are consistent with the work of Krieger *et al.* (2018), in which the simultaneous substitution of seven SRS-amino acids, including position 373, impacted CYP71AZ4 substrate specificity. This suggests residue 373 may contribute to substrate specificity in multiple P450 subfamilies. In the CYP71B subfamily, UMBH enzymes possess an alanine in position 373, while 5OHXS possess a glycine (Fig. 5a). However, substituting CYP71B129 A373 by a glycine did not allow xanthotoxin metabolization, while substituting CYP71B131a G373 by an alanine was not enough to suppress the 5OHXS activity. Taken together, our results allow us to conclude that the acquisition of the 5OHXS activity in the CYP71Bs, CYP71AZs, CYP82Cs and CYP82Ds was made possible by the substitution of different sets of amino acids in each subfamily, tailored per enzymatic environment. Amongst these substitutions, the only constant through the four subfamilies is G373. This means that each enzyme subfamily took a different evolutive path leading to the 5OHXS activity, but along each path, G373 was found to be favorable to xanthotoxin metabolization. Although not indispensable, G373 has thus played a key role in the independent emergence of the 5OHXS activity in different P450 subfamilies.

Residue 373 exerts a significant influence on substrate selectivity for planar molecules, including coumarins and furanocoumarins, based on their longitudinal dimensions within the CYP71B131a context. The consistent emergence of this residue among 5OHXS enzymes across distant botanical families indicates the presence of a potential substrate selectivity hotspot. In the psoralen synthase CYP71AJ1, the residue A362, which position is equivalent to that of CYP71B131a G373, also appeared to play an important role by stabilizing the marmesin substrate in a similar longitudinal orientation (Larbat *et al.*, 2007). By contrast, in the marmesin synthase CYP76F112, the demethylsuberosin substrate adopts a distinct binding orientation, reflecting an alternative substrate stabilization mode (Villard *et al.*, 2021). We suggest that such selectivity hotspots may exist broadly within P450 catalytic sites. Although this hypothesis requires careful validation and context-specific evaluation, it holds potential for advancing the functional characterization of P450 enzymes with convergent functions across distant taxa, particularly in the light of the fast development of artificial intelligences such as AlphaFold and other deep-docking approaches (Gentile *et al.*, 2020; Jumper *et al.*, 2021).

From a different perspective, phylogenetic analyses indicated that the 5OHXS activity emerged recently in the Moraceae family, through a lineage-specific CYP71Bs diversification. This evolutionary pattern is similar to that of CYP76F112, the *F. carica* marmesin synthase (Villard *et al.*, 2021). When CYP76F112 was identified, the only Moraceous genomes available were from *Ficus* and *Morus*. By including recent *Artocarpus* and *Antiaris* genomes, we could strengthen and complete previous hypotheses. Indeed, the Moraceae family is divided into two clades (Fig. 5b): the first one consists of the Moreae (e.g. *Morus*) and Artocarpeae (e.g. *Artocarpus*) tribes (Gardner *et al.*, 2021), in which furanocoumarins were never reported. The second clade comprises five tribes, including the Dorstenieae (e.g. *Dorstenia*), Olmedieae (e.g. *Antiaris*) and Ficeae (e.g. *Ficus*), in which furanocoumarins were identified (Gottlieb *et al.*, 1972; Rovinski *et al.*, 1987; Heinke *et al.*, 2011; Shi *et al.*, 2014; Takahashi *et al.*, 2017). This clade will be defined as the furanocoumarin-producing clade. The lack of *5OHXS* genes in both *Morus* and *Artocarpus* supports the hypothesis that *Ficus* furanocoumarin-biosynthetic genes emerged after the *Ficus-Morus* divergence (Villard *et al.*, 2021). The presence of orthologous *5OHXS* genes in *Ficus* and *Antiaris* indicates the 5OHXS activity emerged before the Ficeae-Olmedieae divergence. This strongly suggests that furanocoumarins were absent in the most recent *Ficus-Morus* ancestor but produced by the Ficeae-Olmedieae one. Based on these patterns, it is reasonable to infer that furanocoumarins emerged only once in Moraceae, during the early evolution of the furanocoumarin-producing clade. However, as metabolic and genetic data is still scarce in this plant family, we cannot yet rule out the possibility of a multiple and independent emergence of furanocoumarins in the Dorstenieae tribe and in the Ficeae-Olmedieae subclade, respectively. Additional metabolomic and genetic resources will thus be necessary to completely elucidate furanocoumarin emergence in Moraceae.

Acknowledgements

The authors warmly thank Jessica Amaral (Universidade Federal de Sao Carlos, Brasil), Sakihito Kitajima, (Kyoto Institute of Technology, Japan), Jérémy Grosjean, Sophie Rahuel Clermont and Marwa Roumani (Université de Lorraine, France) for their precious help on the project, including supply in pyranocoumarins standards, access to *Ficus carica* transcriptomic data, and support in mathematical and phytochemical analysis as well as for

molecular biology. The authors also address special thanks to Éléanore Lacoste, Anne-Flore Didelot, Coralie Deschamps, Yann Moreno, Hugo Schitterer, Juliette Braganti-Coral, Camille Chassin, Jeanne Couderc and Bleuenn Suard students of the Biotechnology specialization of ENSAIA, for their investment in the phylogenetic studies, CYP71B129-131 cloning, and their inputs on P450 expression. Plants were grown on the Plant Experimental Platform in Lorraine (PEPLor, Université de Lorraine, France), metabolomic analyses were conducted on the Metabolomic and Structural Analytic Platform (PASM, Université de Lorraine, France). AB was financially supported by a PhD grant provided by the French Governement and Grand Est Region. AB benefited from the mobility program DREAM provided by 'Lorraine Université d'Excellence', funded by the ANR 'Investissements d'avenir' (grant no. 15-004).

Competing interests

None declared.

Author contributions

AB, AO and CC realized the biochemical experiments. CV identified the coding sequences. CV and DRN performed phylogenetic analyses. AB and RK realized the computational structural biology. AB, CV, RL and AH wrote the article. JT, RL and AH supervised the project.

ORCID

Alexandre Bouillé https://orcid.org/0009-0004-8620-0413
Clément Charles https://orcid.org/0009-0009-0343-1061
Alain Hehn https://orcid.org/0000-0003-4507-8031
Rashmi Kumari https://orcid.org/0000-0001-9886-3231
Romain Larbat https://orcid.org/0000-0002-9060-5040
David R. Nelson https://orcid.org/0000-0003-0583-5421
Alexandre Olry https://orcid.org/0000-0002-2008-9845
Janet Thornton https://orcid.org/0000-0003-0824-4096
Cloé Villard https://orcid.org/0000-0001-6683-8541

Data availability

Nucleotide sequences coding for CYP71B129, CYP71B130 and CYP71B131a are openly available on EnsemblPlants (https://plants.ensembl.org/index.html) under accession nos. FCD_00002714, FCD_00002719 and FCD_00002721 from the genome assembly UNIPI_FiCari_1.0.

References

Abegaz BM, Ngadjui BT, Folefoc GN, Fotso S, Ambassa P, Bezabih M, Dongo E, Rise F, Petersen D. 2004. Prenylated flavonoids, monoterpenoid furanocoumarins and other constituents from the twigs of *Dorstenia elliptica* (Moraceae). *Phytochemistry* **65**: 221–226.

Benson DA, Cavanaugh M, Clark K, Karsch-Mizrachi I, Lipman DJ, Ostell J, Sayers EW. 2012. GenBank. *Nucleic Acids Research* **41**: D36–D42.

Daniel L, Buryska T, Prokop Z, Damborsky J, Brezovsky J. 2015. Mechanism-based discovery of novel substrates of haloalkane dehalogenases using *in silico* screening. *Journal of Chemical Information and Modeling* **55**: 54–62.

DeLano WL. 2002. *PyMOL: an open-source molecular graphics tool.*

Dueholm B, Krieger C, Drew D, Olry A, Kamo T, Taboureau O, Weitzel C, Bourgaud F, Hehn A, Simonsen HT. 2015. Evolution of substrate recognition sites (SRSs) in cytochromes P450 from Apiaceae exemplified by the CYP71AJ subfamily. *BMC Evolutionary Biology* **15**: 122.

Gardner EM, Garner M, Cowan R, Dodsworth S, Epitawalage N, Arifiani D, Sahromi BWJ, Forest F, Maurin O *et al.* 2021. Repeated parallel losses of inflexed stamens in Moraceae: phylogenomics and generic revision of the tribe Moreae and the reinstatement of the tribe Olmedieae (Moraceae). *Taxon* **70**: 946–988.

Gentile F, Agrawal V, Hsing M, Ton A-T, Ban F, Norinder U, Gleave ME, Cherkasov A. 2020. Deep docking: a deep learning platform for augmentation of structure based drug discovery. *ACS Central Science* **6**: 939–949.

Gotoh O. 1992. Substrate recognition sites in cytochrome P450 family 2 (CYP2) proteins inferred from comparative analyses of amino acid and coding nucleotide sequences. *Journal of Biological Chemistry* **267**: 83–90.

Gottlieb OR, Da Silva ML, Maia JGS. 1972. Distribution of coumarins in Amazonian Brosimum species. *Phytochemistry* **11**: 3479–3480.

Gu M, Wang M, Guo J, Shi C, Deng J, Huang L, Huang L, Chang Z. 2019. Crystal structure of CYP76AH1 in 4-PI-bound state from *Salvia miltiorrhiza*. *Biochemical and Biophysical Research Communications* **511**: 813–819.

Hansen CC, Sørensen M, Veiga TAM, Zibrandtsen JFS, Heskes AM, Olsen CE, Boughton BA, Møller BL, Neilson EHJ. 2018. Reconfigured cyanogenic glucoside biosynthesis in *Eucalyptus cladocalyx* involves a cytochrome P450 CYP706C55. *Plant Physiology* **178**: 1081–1095.

Hebsgaard S. 1996. Splice site prediction in *Arabidopsis thaliana* pre-mRNA by combining local and global sequence information. *Nucleic Acids Research* **24**: 3439–3452.

Hehmann M, Lukacin R, Ekiert H, Matern U. 2004. Furanocoumarin biosynthesis in *Ammi majus* L.: cloning of bergaptol O-methyltransferase. *European Journal of Biochemistry* **271**: 932–940.

Heinke R, Franke K, Porzel A, Wessjohann LA, Awadh Ali NA, Schmidt J. 2011. Furanocoumarins from *Dorstenia foetida*. *Phytochemistry* **72**: 929–934.

Hodgson H, De La Peña R, Stephenson MJ, Thimmappa R, Vincent JL, Sattely ES, Osbourn A. 2019. Identification of key enzymes responsible for protolimonoid biosynthesis in plants: opening the door to azadirachtin production. *Proceedings of the National Academy of Sciences, USA* **116**: 17096–17104.

Irmisch S, Clavijo McCormick A, Günther J, Schmidt A, Boeckler GA, Gershenzon J, Unsicker SB, Köllner TG. 2014. Herbivore-induced poplar cytochrome P450 enzymes of the CYP71 family convert aldoximes to nitriles which repel a generalist caterpillar. *The Plant Journal* **80**: 1095–1107.

Ji J, Han X, Zang L, Li Y, Lin L, Hu D, Sun S, Ren Y, Maker G, Lu Z *et al.* 2024. Integrative multi-omics data elucidating the biosynthesis and regulatory mechanisms of furanocoumarins in *Angelica dahurica*.

Jumper J, Evans R, Pritzel A, Green T, Figurnov M, Ronneberger O, Tunyasuvunakool K, Bates R, Žídek A, Potapenko A *et al.* 2021. Highly accurate protein structure prediction with AlphaFold. *Nature* **596**: 583–589.

Karamat F, Olry A, Munakata R, Koeduka T, Sugiyama A, Paris C, Hehn A, Bourgaud F, Yazaki K. 2014. A coumarin-specific prenyltransferase catalyzes the crucial biosynthetic reaction for furanocoumarin formation in parsley. *The Plant Journal* 77: 627–638.

Katoh K, Rozewicki J, Yamada KD. 2019. MAFFT online service: multiple sequence alignment, interactive sequence choice and visualization. *Briefings in Bioinformatics* **20**: 1160–1166.

Kitajima S, Aoki W, Shibata D, Nakajima D, Sakurai N, Yazaki K, Munakata R, Taira T, Kobayashi M, Aburaya S *et al.* 2018. Comparative multi-omics analysis reveals diverse latex-based defense strategies against pests among latex-producing organs of the fig tree (*Ficus carica*). *Planta* **247**: 1423–1438.

Kokina A, Kibilds J, Liepins J. 2014. Adenine auxotrophy – be aware: some effects of adenine auxotrophy in *Saccharomyces cerevisiae* strain W303-1A. *FEMS Yeast Research* **14**: 697–707.

Krieger C, Roselli S, Kellner-Thielmann S, Galati G, Schneider B, Grosjean J, Olry A, Ritchie D, Matern U, Bourgaud F *et al.* 2018. The CYP71AZ P450

subfamily: a driving factor for the diversification of coumarin biosynthesis in apiaceous plants. *Frontiers in Plant Science* **9**: 820.

Kruse T, Ho K, Yoo H-D, Johnson T, Hippely M, Park J-H, Flavell R, Bobzin S. 2008. In planta biocatalysis screen of P450s identifies 8-Methoxypsoralen as a substrate for the CYP82C subfamily, yielding original chemical structures. *Chemistry & Biology* **15**: 149–156.

Kuraku S, Zmasek CM, Nishimura O, Katoh K. 2013. aLeaves facilitates on-demand exploration of metazoan gene family trees on MAFFT sequence alignment server with enhanced interactivity. *Nucleic Acids Research* **41**: W22–W28.

Larbat R, Kellner S, Specker S, Hehn A, Gontier E, Hans J, Bourgaud F, Matern U. 2007. Molecular cloning and functional characterization of psoralen synthase, the first committed monooxygenase of furanocoumarin biosynthesis. *Journal of Biological Chemistry* **282**: 542–554.

Limones-Mendez M, Dugrand-Judek A, Villard C, Coqueret V, Froelicher Y, Bourgaud F, Olry A, Hehn A. 2020. Convergent evolution leading to the appearance of furanocoumarins in citrus plants. *Plant Science* **292**: 110392.

Ma B, Luo Y, Jia L, Qi X, Zeng Q, Xiang Z, He N. 2014. Genome-wide identification and expression analyses of cytochrome *P450* genes in mulberry (*Morus notabilis*). *Journal of Integrative Plant Biology* **56**: 887–901.

Mamoucha S, Fokialakis N, Christodoulakis NS. 2016. Leaf structure and histochemistry of *Ficus carica* (Moraceae), the fig tree. *Flora – Morphology, Distribution, Functional Ecology of Plants* **218**: 24–34.

Mirdita M, Schütze K, Moriwaki Y, Heo L, Ovchinnikov S, Steinegger M. 2022. ColabFold: making protein folding accessible to all. *Nature Methods* **19**: 679–682.

Moore BM, Wang P, Fan P, Leong B, Schenck CA, Lloyd JP, Lehti-Shiu MD, Last RL, Pichersky E, Shiu S-H. 2019. Robust predictions of specialized metabolism genes through machine learning. *Proceedings of the National Academy of Sciences, USA* **116**: 2344–2353.

Munakata R, Kitajima S, Nuttens A, Tatsumi K, Takemura T, Ichino T, Galati G, Vautrin S, Bergès H, Grosjean J *et al.* 2020. Convergent evolution of the UbiA prenyltransferase family underlies the independent acquisition of furanocoumarins in plants. *New Phytologist* **225**: 2166–2182.

Nelson D, Werck-Reichhart D. 2011. A P450-centric view of plant evolution: P450-centric evolution. *The Plant Journal* **66**: 194–211.

Ono E, Murata J. 2023. Exploring the evolvability of plant specialized metabolism: uniqueness out of uniformity and uniqueness behind uniformity. *Plant and Cell Physiology* **64**: 1449–1465.

Pichersky E, Lewinsohn E. 2011. Convergent evolution in plant specialized metabolism. *Annual Review of Plant Biology* **62**: 549–566.

Pluskal T, Torrens-Spence MP, Fallon TR, De Abreu A, Shi CH, Weng J-K. 2019. The biosynthetic origin of psychoactive kavalactones in kava. *Nature Plants* **5**: 867–878.

Pompon D, Louerat B, Bronine A, Urban P. 1996. Yeast expression of animal and plant P450s in optimized redox environments. *Methods in Enzymology* **272**: 51–64.

Rajniak J, Giehl RFH, Chang E, Murgia I, von Wirén N, Sattely ES. 2018. Biosynthesis of redox-active metabolites in response to iron deficiency in plants. *Nature Chemical Biology* **14**: 442–450.

Ronquist F, Huelsenbeck JP. 2003. MrBayes 3: Bayesian phylogenetic inference under mixed models. *Bioinformatics* **19**: 1572–1574.

Ronquist F, Teslenko M, Van Der Mark P, Ayres DL, Darling A, Höhna S, Larget B, Liu L, Suchard MA, Huelsenbeck JP. 2012. MrBayes 3.2: efficient Bayesian phylogenetic inference and model choice across a large model space. *Systematic Biology* **61**: 539–542.

Roselli S, Olry A, Vautrin S, Coriton O, Ritchie D, Navrot N, Krieger C, Vialart G, Bergès H, Bourgaud F *et al.* 2017. Genomic approach to decipher specialized plant pathways: a case study with furanocoumarins in parsnip. *The Plant Journal* **89**: 1119–1132.

Rovinski JM, Tewalt GL, Sneden AT. 1987. Maquiroside A, a new cytotoxic cardiac glycoside from *Maquira calophylla*. *Journal of Natural Products* **50**: 211–216.

Sarker SD, Nahar L. 2017. Progress in the chemistry of naturally occurring coumarins. In: Kinghorn AD, Falk H, Gibbons S, Kobayashi J, eds. *Progress in the chemistry of organic natural products 106*. Cham, Switzerland: Springer International, 241–304.

Schuhegger R, Nafisi M, Mansourova M, Petersen BL, Olsen CE, Svatoš A, Halkier BA, Glawischnig E. 2006. CYP71B15 (PAD3) catalyzes the final step in camalexin biosynthesis. *Plant Physiology* **141**: 1248–1254.

Shi L-S, Kuo S-C, Sun H-D, Morris-Natschke SL, Lee K-H, Wu T-S. 2014. Cytotoxic cardiac glycosides and coumarins from *Antiaris toxicaria*. *Bioorganic & Medicinal Chemistry* **22**: 1889–1898.

Stevenson PC, Simmonds MSJ, Yule MA, Veitch NC, Kite GC, Irwin D, Legg M. 2003. Insect antifeedant furanocoumarins from *Tetradium daniellii*. *Phytochemistry* **63**: 41–46.

Takahashi T, Okiura A, Kohno M. 2017. Phenylpropanoid composition in fig (*Ficus carica* L.) leaves. *Journal of Natural Medicines* **71**: 770–775.

Trott O, Olson AJ. 2010. AutoDock Vina: Improving the speed and accuracy of docking with a new scoring function, efficient optimization, and multithreading. *Journal of Computational Chemistry* **31**: 455–461.

Urban P, Mignotte C, Kazmaier M, Delorme F, Pompon D. 1997. Cloning, yeast expression, and characterization of the coupling of two distantly related *Arabidopsis thaliana* NADPH-cytochrome P450 reductases with P450 CYP73A5. *The Journal of Biological Chemistry* **272**: 19176–19186.

Usai G, Mascagni F, Giordani T, Vangelisti A, Bosi E, Zuccolo A, Ceccarelli M, King R, Hassani-Pak K, Zambrano LS *et al.* 2020. Epigenetic patterns within the haplotype phased fig (*Ficus carica* L.) genome. *The Plant Journal* **102**: 600–614.

Vieira IJC, Mathias L, Monteiro VDFF, Braz-Filho R, Rodrigues-Filho E. 1999. A new Coumarln from Brosimum Gaudichaudii Trecul. *Natural Product Letters* **13**: 47–52.

Villard C, Munakata R, Kitajima S, Velzen R, Schranz ME, Larbat R, Hehn A. 2021. A new P450 involved in the furanocoumarin pathway underlies a recent case of convergent evolution. *New Phytologist* **231**: 1923–1939.

Wang K, Zeng H, Dai Y, Wang Z, Tang H, Li J, Lu X, Jiang N, Xie G, Zhu Y *et al.* 2024. Three types of enzymes complete the furanocoumarins core skeleton biosynthesis in *Angelica sinensis*. *Phytochemistry* **222**: 114102.

Weng J-K, Lynch JH, Matos JO, Dudareva N. 2021. Adaptive mechanisms of plant specialized metabolism connecting chemistry to function. *Nature Chemical Biology* **17**: 1037–1045.

Yano JK, Hsu M-H, Griffin KJ, Stout CD, Johnson EF. 2005. Structures of human microsomal cytochrome P450 2A6 complexed with coumarin and methoxsalen. *Nature Structural & Molecular Biology* **12**: 822–823.

Yu J, Ke T, Tehrim S, Sun F, Liao B, Hua W. 2015. PTGBase: an integrated database to study tandem duplicated genes in plants. *Database* **2015**: bav017.

Zuntini AR, Carruthers T, Maurin O, Bailey PC, Leempoel K, Brewer GE, Epitawalage N, Françoso E, Gallego-Paramo B, McGinnie C *et al.* 2024. Phylogenomics and the rise of the angiosperms. *Nature* **629**: 843–850.

Supporting Information

Additional Supporting Information may be found online in the Supporting Information section at the end of the article.

Fig. S1 Nucleotide dataset of *Ficus carica* and *Morus notabilis* CYP71 clan sequences.

Fig. S2 Protein sequence alignment of *Ficus carica* and *Morus notabilis* CYP71 clan sequences.

Fig. S3 Evaluation of the expression of CYP71Bs and associated mutants by immunodetection.

Fig. S4 Nucleotide sequence alignment of CYP71Bs from the nitrogen-fixing clade.

Fig. S5 Phylogeny of the CYP71B tribe in the nitrogen-fixing clade.

Fig. S6 Restricted nucleotide sequence alignment of CYP71Bs from the Moraceae family.

Fig. S7 Formal identification of the xanthotoxin metabolization product by CYP71B131a_G373A and CYP71B131a_G373S.

Fig. S8 Determination of the optimal temperature of 5-hydroxyxanthotoxin synthases.

Fig. S9 Determination of the optimal pH of 5-hydroxyxanthotoxin synthases.

Fig. S10 Affinity of various CYP71Bs for xanthotoxin and umbelliferone.

Fig. S11 Protein sequence comparison of characterized 5-hydroxyxanthotoxin synthases (5OHXSs) and closely related enzymes.

Fig. S12 Metabolism of xanthotoxin (a) and umbelliferone (b) by CYP71B129, CYP71B130, CYP71B131a, their mutants, and the empty plasmid in the presence (+) or absence (−) of the NADPH cofactor.

Fig. S13 Formal identification of the umbelliferone metabolization product by CYP71B mutants.

Table S1 Substrates tested for CYP71B129–131a functional screening.

Table S2 Comparison of the *Ficus carica* and *Morus notabilis* CYPomes.

Table S3 CYP71Bs from the nitrogen-fixing clade.

Please note: Wiley is not responsible for the content or functionality of any Supporting Information supplied by the authors. Any queries (other than missing material) should be directed to the *New Phytologist* Central Office.

Disclaimer: The New Phytologist Foundation remains neutral with regard to jurisdictional claims in maps and in any institutional affiliations.